Insights gained into the interpretation of surface electromyograms from the gastrocnemius muscles: A simulation study

Title: Insights gained into the interpretation of surface electromyograms from the gastrocnemius muscles: a simulation study.

Authors: Luca Mesin[1], Roberto Merletti[2] and Taian M.M. Vieira[2,3]

1 – Department of Electronics, Politecnico di Torino, Torino, Italy.

2 - Laboratory for Engineering of the Neuromuscular System, Politecnico di Torino, Torino, Italy.

3 - School of Physical Education and Sports, Federal University of Rio de Janeiro, Rio de Janeiro, Brazil.

Keywords: Electromyography, EMG Modeling, Volume Conductor, Pinnate Muscle

Word count: 3247

Corresponding author:

Taian Vieira

Dipartimento di Elettronica, Politecnico di Torino

Corso Duca degli Abruzzi 24, Torino, 10129 ITALY

Tel: 0039-011-4330476

Fax: 0039-0114330404

e-mail: taian.vieira@delen.polito.it

ABSTRACT

Interpretation of surface electromyograms (EMG) is usually based on the assumption that the surface representation of action potentials does not change during their propagation. This assumption does not hold for muscles whose fibers are oblique to the skin. Consequently, the interpretation of surface EMGs recorded from pinnate muscles unlikely prompts from current knowledge. Here we present a complete analytical model that supports the interpretation of experimental EMGs detected from muscles with oblique architecture. EMGs were recorded from the medial gastrocnemius muscle during voluntary and electrically elicited contractions. Preliminary indications obtained from simulated and experimental signals concern the spatial localization of surface potentials and the myoelectric fatigue. Specifically, the spatial distribution of surface EMGs was localized about the fibers superficial extremity. Strikingly, this localization increased with the pinnation angle, both for the simulated EMGs and the recorded M-waves. Moreover, the average rectified value (ARV) and the mean frequency (MNF) of interference EMGs increased and decreased with fatigue, respectively. Furthermore, the degree of variation in ARV and MNF did not depend on the pinnation angle simulated. Similar variations were observed for the experimental EMGs, although being less evident for a higher fiber inclination. These results are discussed on a physiological context, highlighting the relevance of the model proposed here for the interpretation of gastrocnemius EMGs and for conceiving future experiments on muscles with pinnate geometry.

1. INTRODUCTION

The modeling of surface electromyograms (EMGs) has been sought for the interpretation of experimental data (Dimitrova and Dimitrov 2003; Merletti et al., 1999b; Roeleveld et al., 1997), for the development of algorithms aimed at information extraction (Duchene and Hogrel, 2000; Mesin et al., 2009), and for didactic purposes (Merletti et al., 1999a). Available models for the generation of surface EMGs rely both on numerical (Lowery et al., 2004; Mesin et al., 2006) and analytical (Block et al., 2002; Farina et al., 2004b;Gootzen et al., 1991; Mesin, 2006) approaches.

The assumption that the volume conductor is invariant in the direction of propagation of intracellular action potentials allowed for the development of fast analytical models for the simulation of surface EMGs (Farina and Merletti, 2001; Farina et al., 2004a). If a volume conductor is space invariant, the surface representation of a motor unit action potential does not change with its propagation. Such space invariance is frequently assumed when simulating, processing and interpreting experimental EMGs (Lindstrom and Magnusson, 1977; Reucher et al., 1987). Therefore, much of the insights gained into the interpretations of surface EMGs from the use of mathematical models are valid, exclusively, for muscles whose geometry fits in the assumption of space invariance.

Some of the muscles investigated by surface EMG cannot be approximated assuming the muscle fibers to be parallel to the skin. The fibers of the gastrocnemius muscle, for example, are inclined with respect to the skin surface and extend from the deep to the superficial aponeurosis (Kawakami et al, 1998; Narici et al., 1996). Surface electrodes positioned on the calf are, thus, located above the superficial aponeurosis, where muscle fibers attach. Considering that action potentials propagate along the muscle fibers, their propagation along the oblique gastrocnemius fibers contributes to the surface EMGs with a component toward muscle extremities and another toward the skin/tibia. Therefore, the area on the skin surface upon which the action potential of a single muscle fiber

distributes likely depends on how inclined the muscle fibers are (i.e. its pinnation angle) (Vieira et al., 2011). Currently existing models do not provide indications of how the surface EMG relates to the pinnation angle. Which physiologically relevant information might be extracted from surface EMGs in the pinnate gastrocnemius muscle is unknown.

In this study we simulate a pinnate muscle, with fibers inclined in the depth direction, to interpret surface EMGs detected from the gastrocnemius muscles. A complete mathematical model, which includes muscle fibers with finite length and three layers of tissues, is presented here for the generation of single fiber action potentials (SFAP). In particular, we simulate the distribution of motor unit action potentials (MUAPs) on the skin and the interference EMG for different degrees of inclination of muscle fibers. The implications for the interpretation of how action potentials distribute on the skin surface and for the estimation of muscle fatigue are addressed as well. Ultrasound images and experimental EMGs are recorded from the human medial gastrocnemius (MG) muscle to investigate how much theoretical and empirical data correspond.

2. METHODS

2.1 Mathematical model

The simulation model was developed by extending our previous work (Mesin and Farina, 2004), which considered the impulse response of a two layer volume conductor. Three layers were considered here (skin, fat and muscle; figure 1). Moreover a complete model (including finite-length fibers) was implemented to generate single fiber action potentials (SFAP).

Figure 1

Libraries of MUAPs were generated from the simulated SFAPs. These libraries were used with a model of spatial and temporal recruitment of motor units (MUs) to simulate interference EMGs during fatiguing contractions.

Full details on the model and the simulated EMGs are described in the Appendix.

2.2 Experimental signals

Single-differential EMGs were recorded from the medial gastrocnemius (MG) muscle to test for the correctness of the information gained from simulated signals. In particular, we investigated how the amplitude of surface potentials varies with the pinnation angle. This is of remarkable interest since this variation likely provides information of how localized the gastrocnemius activity might be. Moreover, we were interested in understanding whether experimental and simulated EMGs in pinnate muscles are comparable during fatiguing contractions.

Three male subjects (age: 33, 29, 27years; body mass: 78, 80, 75kg; height: 182, 178, 180cm) participated in two protocols designed to compare experimental and simulated signals.

Protocol 1: Sixteen surface electrodes (10 mm IED) were used to record EMGs during electrical stimulation. Two ankle angles were considered; foot in neutral position (~20^o pinnation angle) and plantar flexed (~35^o pinnation angle). With an adhesive pre-gelled electrode (cathode; figure 6a) placed carefully on the leg, bipolar current pulses were delivered at 2 pps and for 20s to the tibial posterior nerve. The anode electrode (80 × 50 mm; soaked cloth) was positioned immediately above the patella with elastic Velcro straps. Stimulation amplitude was as minimal as possible to allow for the detection of the firstly observable M-wave. Low stimulation amplitude was chosen to recruit the least number of MUs and, thus, to better isolate the effect of ankle angle on the distribution of M-waves amplitude on the skin. Averaged M-waves were obtained after triggering the 15 single-differential EMGs.

Protocol 2: EMGs were recorded with an array of eight electrodes (5mm interelectrode distance – IED) when the subjects exerted isometric plantar flexion at 60% MVC. The contraction lasted for

30s to ensure the occurrence of myoelectric manifestation of fatigue. Fatigue plots were created from the average rectified value (ARV) and the mean frequency (MNF) calculated on 500ms epochs (i.e. both descriptors are plotted with respect to their initial values). ARV and MNF indices were calculated as indicated in Merletti et al. 1990. This protocol was applied once with the foot dorsal flexed (pinnation angle ~10°) and once in neutral position (pinnation angle ~20°), with 5 min interval between trials. Plantar flexion torque was measured and displayed to the subjects. Subjects were in prone position and their feet were firmly secured to a footplate, with the lateral malleolus being coaxial to the centre of rotation of the torque meter. MVC values were determined for each pinnation angle as the maximum torque measured across three attempts separated by 5 minutes.

EMGs were amplified (gain ranged from 1k to 5k; 10–500 Hz EMG-USB amplifier, LISiN and OTBioelettronica, Turin), and sampled at 2048 Hz with a 12bit A/D converter (±2.5V dynamic range). Ultrasound images were taken with a linear probe (3.86 cm long; Fukuda Denshi, UF 4000, 7.5 MHz) and pinnation angles were estimated with the precision of one degree. A custom-made neuromuscular stimulator (LISiN, Turin), equipped with a hybrid output stage, was used in the first protocol. In the second protocol, load cells output was amplified (150Nm full-scale amplifier; MISOII, OTBioelettronica, Turin) and then converted to values of ankle torque. After cleansing of the skin with abrasive paste and water, ultrasound scanning was used to place electrodes on the MG muscle. Specifically, electrodes were positioned above the sheath of aponeurotic tissue and parallel to the surface projection of the pinnate MG fascicles. Care was taken to ensure that the array and the ultrasound probe had similar orientation, which provided an ultrasound image with as many fascicles as possible.

3. RESULTS

3.1 Preliminary Simulations

Some preliminary simulations are shown in figures 2 and 3, in order to compare the surface potentials produced by fibers with different arrangements (parallel or slightly inclined with respect to the skin). In particular, the potential distribution over the skin surface is considered for fixed time samples in figure 2, whereas the signals detected as functions of time from arrays of electrodes sampling the potential in specific points aligned to the fibers are shown in figure 3.

Simulations showed that the amplitude and the shape of surface potentials change with the obliquity of muscle fibers (figure 2). When simulating fibers parallel to the skin, the surface distribution of action potentials was symmetric with respect to the innervation zone (IZ). Conversely, by increasing the fiber inclination, the surface potential became more asymmetric, as the contribution of the deeper source was attenuated and more diffused than that of the most superficial source. The root mean square (RMS) difference between the surface distribution of potentials simulated for 10° and those computed for the other pinnation angles (0°, 5°, 15°, and 20°) is shown as a function of the source position (figure 2b). As expected, greater RMS differences were obtained for higher variations between angles. The greatest difference occurred when the source was close to the extinction region.

Regardless of whether simulating monopolar or single-differential signals, variations in the amplitude of surface potentials across electrodes depended on the pinnation angle. By simulating an electrode array placed parallel to the x-z projection of a superficial muscle fiber with 0^o pinnation angle, both monopolar and differential potentials appeared with equal amplitudes on either sides from the IZ (left panel in figure 3a). For deep fibers, only the standing waves produced by the generation and extinction of simulated potentials are seen in the EMGs, respectively (right panel in figure 3a). By inclining muscle fibers, the amplitude distribution of surface potentials concentrated progressively more toward the superficial tendon (left panels in figure 3b,c). Interestingly, pinnate fibers simulated 10cm away from the electrodes contributed to the surface EMGs with potentials of

markedly smaller amplitude (3-5 times smaller; right panels in figure 3b,c). Therefore, surface electrodes on pinnate muscles sample only from sources located nearby and nowhere else.

The inclination of muscle fibers affects also the shape and the propagation of surface potentials. Close inspection of figure 3 reveals that the surface potential from fibers parallel to the skin has the same duration, wherever it is sampled on the skin. Propagation of these potentials is also evident in the figure. Potentials from pinnate fibers undergo large shape variations when recorded from different channels, so that conduction velocity (CV) cannot be estimated properly (Farina and Merletti, 2004). Specifically, they have shorter duration when detected closer to the superficial tendon. Moreover, the delay between successive peaks or valleys of potentials simulated for adjacent channels is not the same for pinnate fibers. Then, surface EMGs detected from muscles with fibers not parallel to the skin unlikely show the propagation of action potentials along muscle fibers.

Figures 2 and 3

3.2 Amplitude distribution of EMGs

In figure 4, simulated single fiber potentials are investigated to quantify how much the spatial distribution of surface EMGs changes as a function of the pinnation angle. Surface potentials were compared for volume conductors with various pinnation angles, from 0° to 45°, and for two thicknesses of the fat layer. Contour plots of simulated surface potentials are shown at a given time (figure 4b). To quantify the diffusion of the surface potential, the median and the first and third quartiles were investigated along orthogonal sections of contour plots (figure 4c). The potential generated using a model of parallel fibers was more diffused (interquartile interval: ~40mm) over the skin with respect to that generated with a pinnate geometry (interquartile interval: less than 25mm for pinnation angles higher than 10°; figure 4).

As for the simulated SFAPs, the amplitude distribution of electrically elicited EMGs depended on the degree of inclination of MG fibers. When MG fascicles were ~20° oblique, the firstly emerging M-waves appeared on the most proximal muscle portion, from the channel 1 to 5 (figure 5b). The ARV amplitude of M-waves distributed evenly across these channels (interquartile interval: 53.7mm). Strikingly, for the same stimulation amplitude and higher pinnation angle (~35°), the distribution of ARV amplitude changed chiefly across channels (interquartile interval: 32.2mm), with the most proximal channels detecting the largest M-waves (figure 5c). Additionally, M-waves recorded from the pinnate gastrocnemius muscle showed neither a delay nor a phase opposition between consecutive channels.

Figure 4 and 5

3.3. Simulated and experimental manifestation of fatigue in surface EMGs

Simulations indicate that amplitude and spectral descriptors might be used to study the myoelectric manifestations of fatigue in the pinnate gastrocnemius muscle. Single-differential EMGs, simulated and recorded with seven channels aligned to the longitudinal projection of muscle fibers, are shown for two pinnation angles (10° and 20°; figure 6). Both simulated (session 2.4) and experimental signals showed myoelectric manifestation of fatigue, with ARV and MNF increasing and decreasing with time, respectively (fatigue plots; figure 6). Interestingly, changes in amplitude and frequency were more variable for the experimental EMGs; and this high variability increases with the pinnation angle (Table 1).

Figure 6, Table 1

4. DISCUSSION

A model for the simulation and interpretation of surface EMGs in pinnate muscles is proposed here. Simulations indicate that the obliquity of muscle fibers has a marked effect on the surface EMG (figure 2). The higher the fibers pinnation the more localized was the surface distribution of action potentials, with electrodes closer to the fibers end detecting remarkably higher potentials. This localized distribution of surface potentials is more evident for single-differential than for monopolar

signals, likely due to the higher selectivity of differential derivations. Experimental EMGs from the MG substantiated the predictions posed by our simulations.

While there are architectural differences between skeletal muscles, it seems worthy to ask whether the surface EMGs recorded from pinnate muscles are as informative as those recorded from fusiform muscles. Understanding how the amplitude distribution of surface potentials changes with the pinnation angle and the possibility of using surface EMGs to study muscle fatigue are of particular interest.

4.1 Localization of surface EMGs depends on the pinnation angle of the gastrocnemius muscle

Our simulations revealed that surface electrodes on muscles with fibers not parallel to the skin sample from nearby sources and from nowhere else. This key result is substantiated from our observations that: i) surface potentials were localized over the superficial tendon of pinnate fibers, with the main contribution being due to the extinction phase of intracellular action potentials (figure 3); ii) although the representation of surface potentials was 50% less localized when trebling the fat thickness, it was still considerably more concentrated on the superficial tendon than the surface representation of potentials in parallel fibers (figure 4); iii) two pinnate fibers with distal tendons separated by 10cm produced surface potentials with separated amplitude distributions. Consequently, the pinnation brings a wider cross section of the muscle into the view of surface electrodes than that available for parallel-fibered muscles. It is worth to mention that the localized distribution shown in figures 3 and 4 refers to the amplitude of SFAPs. As the amplitude of MUAPs corresponds to the algebraic summation of several SFAPs, the localized representation of individual MUAPs in the surface EMGs depends on whether MUs have small territories (Vieira et al., 2011), Here, we are not interested on the size of MUs territories but on how much the amplitude distribution of SFAPs changes with the pinnation angle.

Electrical stimulation of the tibial nerve revealed a somewhat similar localization of surface M-waves detected from the MG muscle (figure 5), with respect to that observed for simulated potentials. The smallest stimulation amplitude leading to the first observable M-waves was chosen to ensure that only a few MUs were stimulated. By keeping constant the stimulation amplitude, the effect of pinnation angle on the localization of M-waves was isolated. M-waves with similar amplitude were observed for the four most proximal channels when stimulation pulses were delivered with the foot in neutral position (figure 5b, $\theta = 20°$). With the foot plantar flexed (figure 5c, $\theta = 35°$), the amplitude of M-waves distributed unevenly across the four most proximal channels. Larger M-waves appeared for the more proximal channels. While the variation in ankle joint angle could have induced variation in the stimulation site, as the nerve moves beneath the stimulation electrode, the similitude of EMGs likely indicates that the same population of MUs was stimulated in both foot conditions.

Surface EMGs convey unique information regarding the activation of the pinnate gastrocnemius muscle. In muscles whose fibers are parallel to the skin, surface electrodes detect the propagation of MUAPs (Farina et al, 2002; Merletti et al., 2003). In the gastrocnemius muscle, the amplitude of surface EMGs varies with the number of active fibers beneath the recording electrodes. Very recently, for example, we used the model presented here to validate our estimations of the longitudinal size of MUs territory in the human MG muscle (Vieira et al., 2011). Specifically, we observed that with respect to the MG length, the fibers of individual MUs extended for only a short distance (less than 4cm). Then, activation of individual MUs leads to regional activation of the MG muscle. Indeed, the extensive evidence positing localized activation of the calf muscles in humans and cats is not surprising (Eng and Hoffer, 1997; English and Weeks, 1989; McLean and Goudy, 2004; Staudenmann et al., 2009; Vieira et al., 2010a,b; Wolf et al., 1998). If the nervous system takes advantage of muscle architecture to shape the recruitment of MUs (Kennedy and Cresswell,

2001; Vieira et al., 2011), the high-density surface electromyography (Merletti et al., 2010) could provide a mean to study the regional organization of activity in the pinnate gastrocnemius muscle.

4.2 Myoelectric manifestation of fatigue in pinnate muscles

Testing for the possibility of studying fatigue manifestation in skeletal muscles from the surface EMG is not simple. Several factors affect the muscles undergoing fatigue: 1) different strategies of MU recruitment and firing rate; 2) variations in load sharing between synergistic muscles, especially for those spanning the same joint as soleus and gastrocnemius (McLean and Goudy, 2004); 3) changes in shape of intracellular action potentials (Arabadzhiev et al., 2005); 4) synchronization of MUs (Mesin et al., 2009); 5) variable decrease of CV for muscle fibers of different physiological types (Rainoldi et al., 2008). To keep simulations simple, we considered the same percentage of CV changes for all MUs. Additionally, the same spatial and temporal recruitment of MUs was simulated for two different pinnation angles, so as to isolate the effect of fibers inclination on surface EMGs.

Even though it was not possible to observe the changes in CV directly, it was possible to observe myoelectric manifestations of gastrocnemius fatigue in the amplitude and spectral EMG descriptors. Because of the muscle oblique architecture, and considering the scattering of IZs, the extinction of action potentials at the superficial aponeurosis contributed chiefly to the surface EMGs simulated (figure 3). As a consequence, electrodes located over the aponeurotic layer do not detect the same potential propagating toward either the superficial or deep aponeurosis. Instead, they record standing waves likely resulting from the end-of-fiber effect (Stegeman et al., 1997). This interpretation is supported by spike-triggered EMGs, which did not show physiological delays between surface potentials detected by consecutive electrodes located upon the superficial aponeurosis (Vieira et al., 2011). Thus, estimation of CV, which showed remarkable properties in the investigation of myoelectric fatigue in parallel-fibered muscles (Mesin et al., 2009), cannot be

obtained from the gastrocnemius muscle, at least not upon its superficial aponeurosis. Nevertheless, simulations showed that ARV and MNF of surface EMGs are both affected by variations in CV.

Although at different extents, the experimental and simulated manifestations of fatigue were observed in the pinnate gastrocnemius muscle. Simulations did not show any reliance of the variations in ARV and MNF on the pinnation angle. Nevertheless, the variability of ARV and MNF were different for experimental data recorded for two pinnation angles (Table 1). This suggests that some factors, which were kept constant in the simulations, were involved in the contraction of the MG muscle at different pinnation angles. It has been shown, for example, that variations in activity within and between calf muscles occur when subjects are asked to sustain a low and isometric torque of plantar flexion (McLean and Goudy, 2004; Tamaki et al., 1998). Variable activation within the same gastrocnemius muscle was observed even for different directions of ankle force (Staudenmann et al., 2009) and in quiet standing (Vieira et al., 2010a,b). Considering the more localized distribution of surface potentials for the more oblique geometry (figures 4), and the small territories of gastrocnemius MUs (Vieira et al., 2011), surface electrodes seem to provide very selective recordings for high pinnation angles. Therefore, variations in recruitment and firing rate of MUs during a fatiguing contraction would affect more severely the surface EMGs detected from more oblique MG fibers.

4.3 Future perspectives

The model presented here opens new perspectives for investigating the calf muscles activation, either by supporting the interpretation of experimental data or by providing theoretical grounds upon which future studies will be designed. The surface distribution of simulated action potentials (figures 3 and 4), for example, supports our prediction that postural activation of the MG muscle is organized regionally for the control of quiet standing posture (Vieira et al., 2010a). Similarly, our

simulation results indicate that amplitude and spectral EMG descriptors could be potentially useful to study fatigue in the gastrocnemius muscle.

5. CONCLUSIONS

A new model for the simulation of surface EMGs in pinnate muscles was developed and applied to interpret experimental data obtained from the gastrocnemius muscles. The most striking result was the localized representation of surface potentials. Because of the gastrocnemius pinnate architecture, simulated EMGs and experimental M-waves were both detected only by few consecutive electrodes. Higher pinnation angles led to more localized potentials. The regional organization of gastrocnemius activity in different motor tasks could, then, be investigated with surface electromyography. The potentiality of the model was also shown for the investigation of myoelectric fatigue with amplitude and spectral indexes. Both descriptors varied during fatigue, either for experimental or simulated EMGs. The greater variability in the amplitude and frequency of experimental EMGs, observed for higher pinnation angles, was likely due to different recruitment strategies.

Conflict of Interest Statement

None of the authors has any conflict of interest concerning the publications of this work.

Acknowledgements

T. Vieira is recipient of a doctoral fellowship from the Brazilian National Research Council (CNPq). This study was supported by the Compagnia di San Paolo and Fondazione Cassa di Risparmio di Torino.

REFERENCES

1. Arabadzhiev, T. I., Dimitrov, G. V. Dimitrova, N. A., 2005. Simulation analysis of the performance of a novel high sensitive spectral index for quantifying M–wave changes during fatigue. Journal of Electromyography and Kinesiology 15, 149–158.
2. Blok, J. H., Stegeman, D. F., van Oosterom, A., 2002. Three-layer volume conductor model and software package for applications in surface electromyography. Annals of Biomedical Engineering 30, 566-577.
3. Dimitrova, N. A., Dimitrov, G. V., 2003. Interpretation of EMG changes with fatigue: facts, pitfalls, and fallacies. Journal of Electromyography and Kinesiology 13, 13-36.
4. Duchene, J., Hogrel, J. Y., 2000. A model of EMG generation. IEEE Transactions on Biomedical Engineering 47, 192-201.
5. Eng, J. J., Hoffer, J. A., 1997. Regional variability of stretch reflex amplitude in the cat medial gastrocnemius muscle during a postural task. Journal of Neurophysiology 78, 1150-1154.
6. English, A. W., Weeks, O. I., 1989. Electromyographic cross-talk within a compartmentalized muscle of the cat. Journal of Physiology 416, 327-336.
7. Enoka, R. M., Fuglevand, A. J., 2001. Motor unit physiology: some unresolved issues. Muscle Nerve 24, 4–17.
8. Farina, D., Fattorini, L., Felici, F., Filligoi, G., 2002. Nonlinear surface EMG analysis to detect changes of motor unit conduction velocity and synchronization. Journal of Applied Physiology 93, 1753-1763.
9. Farina, D., Merletti, R., 2001. A novel approach for precise simulation of the EMG signal detected by surface electrodes. IEEE Transaction on Biomedical Engineering 48, 637-646.
10. Farina, D., Mesin, L., Martina, S., 2004a. Advances in surface EMG signal simulation with analytical and numerical descriptions of the volume conductor. Medical and Biological Engineering and Computing 42, 467-476.

11. Farina, D., Mesin, L., Martina, S., Merletti, R., 2004b. A surface EMG generation model with multi-layer cylindrical description of the volume conductor. IEEE Transaction on Biomedical Engineering 51, 415-426.
12. Farina, D., Merletti, R., 2004. Methods for estimating muscle fiber conduction velocity from surface electromyographic signals. Med. Biol. Eng. Comput., 42, 432–445.
13. Fuglevand, A. J., Winter, D. A., Patla, A. E., 1993. Models of recruitment and rate coding organization in motor-unit pools. Journal of Neurophysiology 70, 2470-2488.
14. Gabriel, S., Lau, R. W., Gabriel, C., 1996. The dielectric properties of biological tissues: II. Measurements in the frequency range 10 Hz to 20 GHz. Physics in Medicine and Biology 41, 2251-2269.
15. Gootzen, T. H., Stegeman, D. F., Van Oosterom, A., 1991. Finite limb dimensions and finite muscle length in a model for the generation of electromyographic signals. Electroencephalography and Clinical Neurophysiology 81, 152-162.
16. Heringa, A., Stegeman, D. F., Uijen, G. J., de Weerd, J. P., 1982. Solution methods of electrical field problems in physiology. IEEE Transactions on Biomedical Engineering 29, 34-42.
17. Kawakami, Y., Ichinose, Y., Fukunaga, T., 1998. Architectural and functional features of human triceps surae muscles during contraction. Journal of Applied Physiology 85, 398-404.
18. Kennedy, P. M., Cresswell, A. G., 2001. The effect of muscle length on motor-unit recruitment during isometric planter flexion in humans. Experimental Brain Research 137, 58-64.
19. Lindstrom, L., Magnusson, R., 1977. Interpretation of myoelectric power spectra: A model and its applications. Proceedings of the IEEE 65, 653-662.
20. Lowery, M. M., Stoykov, N. S., Dewald, J. P., Kuiken, T. A., 2004. Volume conduction in an anatomically based surface EMG model. IEEE Transaction on Biomedical Engineering 51, 2138-2147.

21. McLean, L., Goudy, N., 2004. Neuromuscular response to sustained low-level muscle activation: within- and between-synergist substitution in the triceps surae muscles. European Journal of Applied Physiology 91, 204-216.
22. Merletti, R., Aventaggiato, M., Botter, A., Holobar, A., Marateb, H., Vieira, T. M. M., 2010. Advances in surface EMG: Recent progress in detection and processing techniques. Critical Reviews in Biomedical Engineering 38, 305-345.
23. Merletti, R., Farina, D., Gazzoni, M., 2003. The linear electrode array: a useful tool with many applications. Journal of Electromyography and Kinesiology 13, 37-47.
24. Merletti, R., Knaflitz, M., De Luca, C. J., 1990. Myoelectric manifestations of fatigue in voluntary and electrically elicited contractions. Journal of Applied Physiology 69, 1810-1820.
25. Merletti, R., Lo Conte, L., Avignone, E., Guglielminotti, P., 1999a. Modeling of surface EMG signals. Part I: model and implementation. IEEE Transaction on Biomedical Engineering 46, 810-820.
26. Merletti, R., Roy, S. H., Kupa, E., Roatta, S., Granata, A., 1999b. Modeling of surface myoelectric signals Part II: Model-based signal interpretation. IEEE Transaction on Biomedical Engineering 46, 821-829.
27. Mesin, L., 2006. Simulation of Surface EMG Signals for a Multi-layer Volume Conductor with Triangular Model of the Muscle Tissue. IEEE Transactions on Biomedical Engineering 53, 2177-2184.
28. Mesin, L., Cescon, C., Gazzoni, M., Merletti, R., Rainoldi, A., 2009. A new method to estimate myoelectric manifestations of muscle fatigue. Journal of Electromyography and Kinesiology 19, 851-863.
29. Mesin, L., Farina, D., 2004. Simulation of surface EMG signals generated by muscle tissues with in-homogeneity due to fiber pinnation. IEEE Transactions on Biomedical Engineering 51, 1521-1529.

30. Mesin, L., Joubert, M., Hanekom, T., Merletti, R., Farina, D., 2006. A Finite Element Model for Describing the Effect of Muscle Shortening on Surface EMG. IEEE Transactions on Biomedical Engineering 53, 593-600.
31. Narici, M. V., Binzoni, T., Hiltbrand, E., Fasel, J., Terrier, F., Cerretelli, P., 1996. In vivo human gastrocnemius architecture with changing joint angle at rest and during graded isometric contraction. Journal of Physiology 496, 287-297.
32. Rainoldi, A., Gazzoni, M., Melchiorri, G., 2008. Differences in myoelectric manifestations of fatigue in sprinters and long distance runners. Physiological Measurements 29, 331-340.
33. Reucher, H., Silny, J., Rau, G., 1987. Spatial filtering of noninvasive multielectrode EMG: Part II Filter performance in theory and modeling. IEEE Transactions on Biomedical Engineering 34, 106-113.
34. Roeleveld, K., Blok, J. H., Stegeman, D. F., van Oosterom, A., 1997. Volume conduction models for surface EM: confrontation with measurements. Journal of Electromyography and Kinesiology 7, 221-232.
35. Rosenfalck, P., 1969. Intra and extracellular fields of active nerve and muscle fibers. A physico-mathematical analysis of different models. Acta Physiologica Scandinavica 321, 1-49.
36. Staudenmann, D., Kingma, I., Daffertshofer, A., Stegeman, D. F., van Dieën, J. H., 2009. Heterogeneity of muscle activation in relation to force direction: A multi-channel surface electromyography study on the triceps surae muscle. Journal of Electromyography and Kinesiology 19, 882-895.
37. Stegeman, D. F., Dumitru, D., King, J. C., Roeleveld, K., 1997. Near and far fields: source characteristics and the conducting medium in neurophysiology. Journal of Clinical Neurophysiology 14, 429-442.
38. Tamaki, H., Kitada, K., Akamine, T., Murata, F., Sakou, T., Kurata, H., 1998. Alternate activity in the synergistic muscles during prolonged low-level contractions. Journal of Applied Physiology 84, 1943-1951.

39. Vieira, T. M. M., Loram, I. D., Muceli, S., Merletti, R., Farina, D., 2011. Postural activation of the human medial gastrocnemius muscle: are the muscle units spatially localised? Journal of Physiology 589, 431-443.
40. Vieira, T. M. M., Merletti, R., Mesin, L., 2010a. Automatic segmentation of surface EMG images: improving the estimation of neuromuscular activity. Journal of Biomechanics 43, 2149-2158.
41. Vieira, T. M. M., Windhorst, U., Merletti, R., 2010b. Is the stabilization of quiet upright stance in humans driven by synchronized modulations of the activity of medial and lateral gastrocnemius muscles? Journal of Applied Physiology 108, 85-97.
42. Wolf, S. L., Ammerman, J., Jann, B., 1998. Organization of responses in human lateral gastrocnemius muscle to specified body perturbations. Journal of Electromyography and Kinesiology 8, 11-21.

Table 1: Variability of the amplitude (ARV) and frequency (MNF) descriptors of experimental and simulated surface EMGs, calculated as the standard deviation of residuals resulting from the fitting of a first order polynomial to the observed data (dashed lines in figure 4).

	Experimental EMGs		Simulated EMGs	
Pinnation angle (deg)	ARV (μV)	MNF (Hz)	ARV (a.u.)	MNF (Hz)
10	67	4.16	4.21	3.61
20	108	4.68	4.20	3.62

FIGURE CAPTIONS

Figure 1 a) Schematic representation of the volume conductor model, including the definition of the coordinate system and the geometry of the simulated muscle fibers. The muscle layer is considered as homogeneous and anisotropic, with fibers inclined with respect to the skin surface. Fat and skin layers are homogeneous and isotropic. b) Ultrasound image of the gastrocnemius, showing the pinnation of muscle fibers. c) Longitudinal section of the simulated volume conductor, indicating the notation used for determining the analytical solution. d) Sampling of the phenomenological model of the transmembrane current proposed in Rosenfalck (1969), using 10 impulse sources.

Figure 2 a) Surface potential generated in muscle fibers with three different pinnation angles (0°, 5°, and 10°). The signals were simulated using the model shown in Figure 1a,c. b) Root mean square (RMS) difference between the EMG map generated for the pinnation angle of 10° and the maps computed for pinnation angles of 0°, 5°, 15°, and 20°. Two different thicknesses of the fat layer were simulated. RMS values are expressed in percentage and as a function of the position of the source (measured as the distance of each of the two transmembrane current sources from the innervation zone).

Figure 3 Simulation of surface EMG signals detected with an electrode array located over the longitudinal projection of a single muscle fiber on the skin surface. Monopolar and single-differential signals are shown for different fibers, corresponding to different pinnation angles or to different positions.

Figure 4 Simulated (a; see Appendix) and experimental (b; see section 2.2) EMGs are shown for two pinnation angles (10° and 20°) during an isometric fatiguing contraction at 60% of maximal voluntary contraction (MVC). Interference EMGs were simulated with the muscle fiber conduction velocity - CV - decreasing by 1%/s of the initial value. The volume conductors simulated and ultrasound images of the MG muscle are shown on top (arrows indicate detection points). The same firing pattern and population of 340 motor units were simulated for two pinnation angles (10° and

20°). A short time epoch of raw signals is depicted in the middle panel. Fatigue plots are shown in the bottom, including averaged rectified values (ARV) and mean frequency (MNF), estimated for epochs of 500 ms duration (n = 60 epochs) and for each pinnation angle. Values were averaged across channels (n = 7 channels). Dashed lines indicate the best linear fitting to ARV and MNF traces, calculated with the least square method.

Figure 5 Spatial distributions of surface potentials as a function of the pinnation angle. a) Longitudinal view of the volume conductors considered. When the pinnation angle is higher than zero, one of the tendons is located at the muscle/fat interface, representing the superficial aponeurosis. The case in which fibers are parallel to the skin surface is also considered, for two muscle depths. b) Contour plots of the rectified value, averaged over time (ARV), of the simulated surface potential, indicating the median and the first and third quartiles for orthogonal sections crossing the location of maximal amplitude. Note the asymmetry of contours for pinnation angles greater than zero; ARV amplitude concentrates close to the fiber end (the superficial aponeurosis). c) Median, first and third quartiles of ARV in the direction longitudinal (x) and transversal (z) to the fibers are shown for different pinnation angles and for two fat layers.

Figure 6 Spatial distribution of single-differential M-waves detected from the medial gastrocnemius (MG) muscle at two pinnation angles. a) Array of 16 surface electrodes, positioned on the MG muscle, and the stimulation electrode, located above the tibial nerve branch supplying the same muscle. Note that the most proximal EMG electrodes were nearer to the stimulation electrode. b) Raw triggered (black traces) and averaged (gray traces) M-waves detected with the foot positioned so as to result in a pinnation angle of about 20°. The ultrasound image obtained with the foot in this same position is shown on the top. c) the same as in b) for ~35° pinnation angle. Note that the stimulation artefact was most evident for the most proximal channels, which were the closest to the cathode electrode.

Fig 1

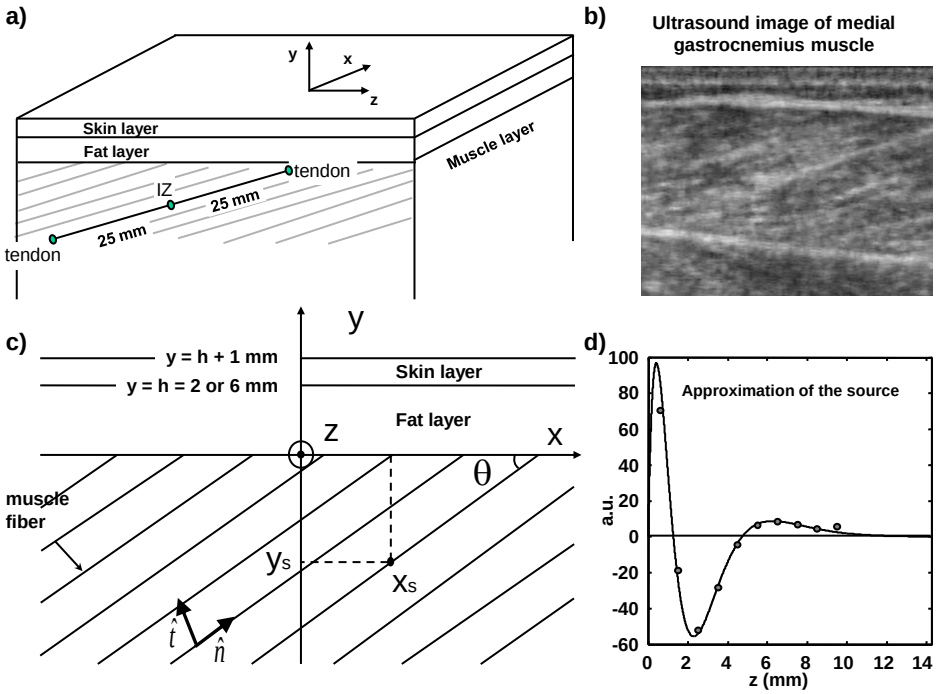
a)
y
x
z
Skin layer
Fat layer
tendon
IZ
25 mm
25 mm
tendon
Muscle layer
b)
Ultrasound image of medial gastrocnemius muscle
c)
y = h + 1 mm
y = h = 2 or 6 mm
Skin layer
Fat layer
z
x
θ
muscle fiber
ys
xs
t̂
n̂
d)
Approximation of the source
a.u.
z (mm)

Fig 2

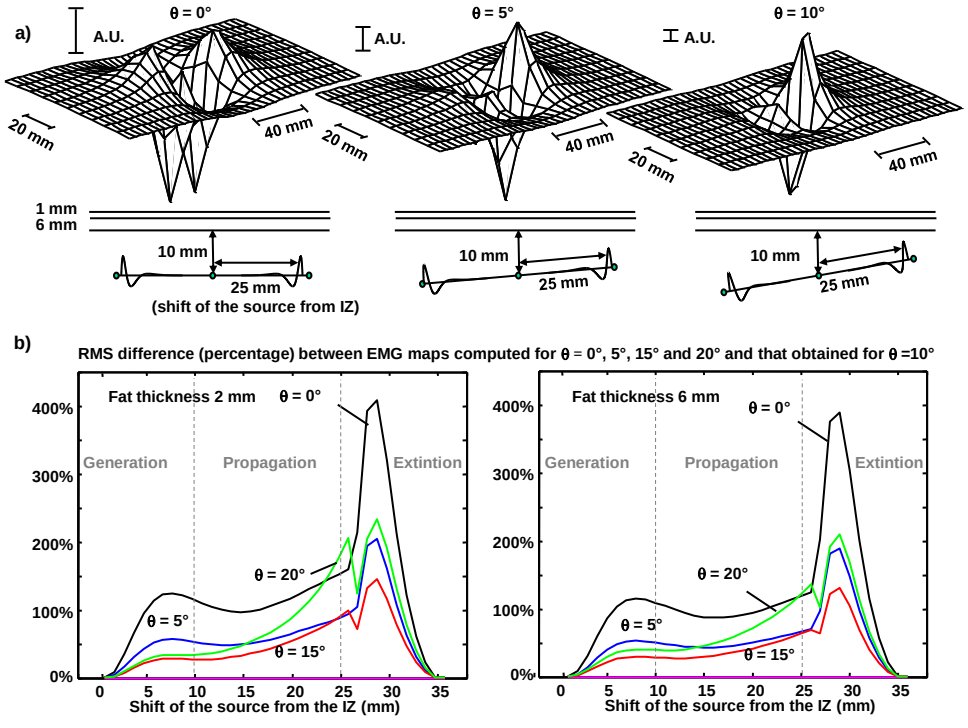
a)
θ = 0°
θ = 5°
θ = 10°
A.U.
20 mm
40 mm
1 mm
6 mm
10 mm
25 mm
(shift of the source from IZ)
b)
RMS difference (percentage) between EMG maps computed for θ = 0°, 5°, 15° and 20° and that obtained for θ =10°
Fat thickness 2 mm
Fat thickness 6 mm
Generation
Propagation
Extintion
θ = 0°
θ = 5°
θ = 15°
θ = 20°
Shift of the source from the IZ (mm)

Fig 3

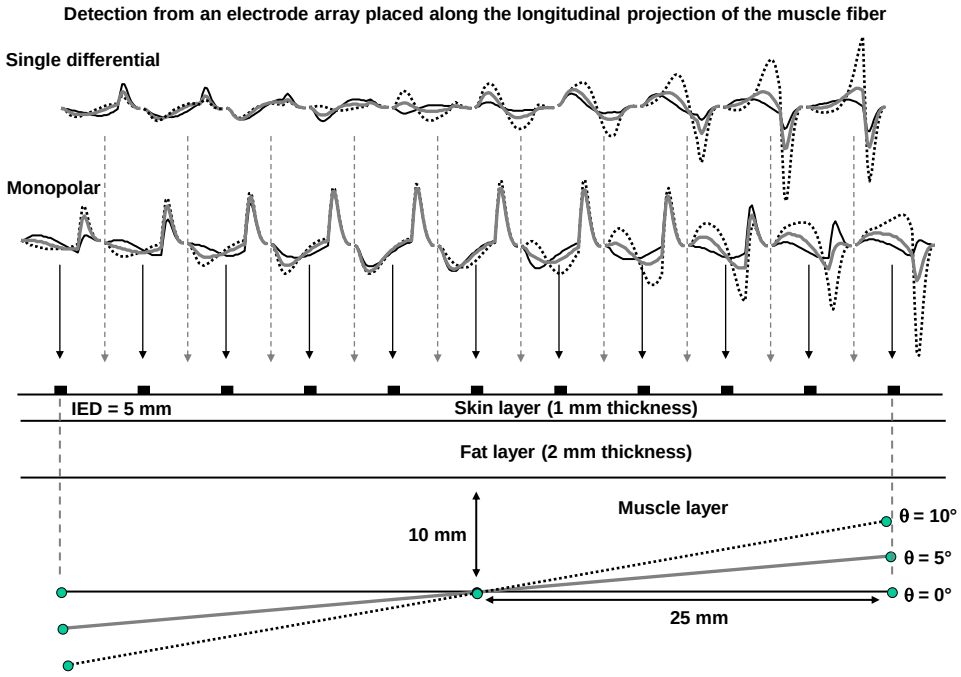
Detection from an electrode array placed along the longitudinal projection of the muscle fiber
Single differential
Monopolar
IED = 5 mm
Skin layer (1 mm thickness)
Fat layer (2 mm thickness)
Muscle layer
10 mm
θ = 10°
θ = 5°
θ = 0°
25 mm

Fig 4

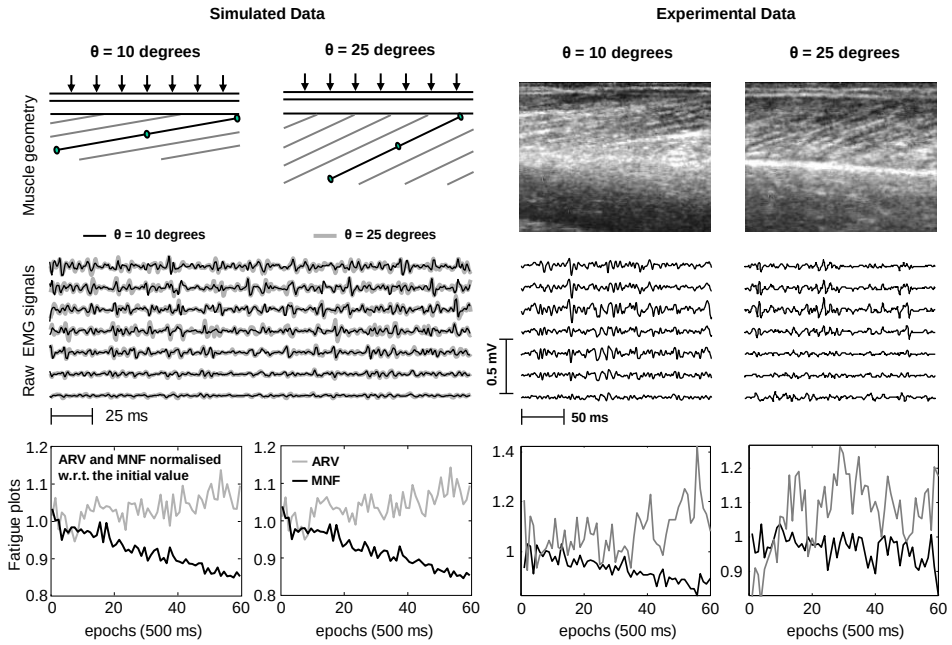
Simulated Data
Experimental Data
θ = 10 degrees
θ = 25 degrees
θ = 10 degrees
θ = 25 degrees
Muscle geometry
θ = 10 degrees
θ = 25 degrees
Raw EMG signals
0.5 mV
25 ms
50 ms
Fatigue plots
ARV and MNF normalised w.r.t. the initial value
ARV
MNF
epochs (500 ms)
epochs (500 ms)
epochs (500 ms)
epochs (500 ms)

Fig 5

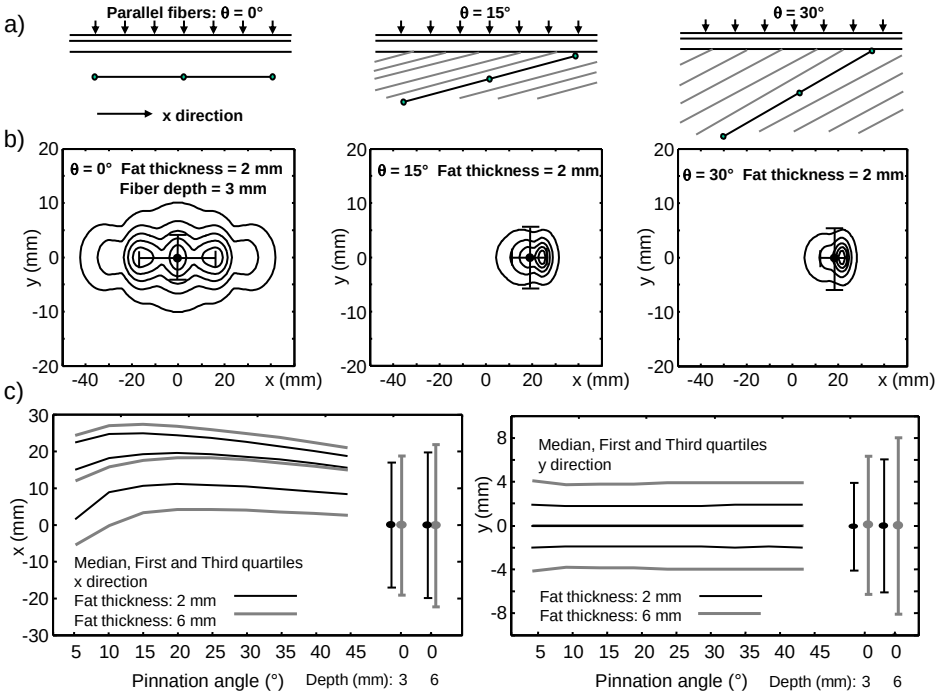
a)
Parallel fibers: θ = 0°
θ = 15°
θ = 30°
x direction
b)
θ = 0° Fat thickness = 2 mm
Fiber depth = 3 mm
θ = 15° Fat thickness = 2 mm
θ = 30° Fat thickness = 2 mm
y (mm)
x (mm)
c)
x (mm)
Median, First and Third quartiles
x direction
Fat thickness: 2 mm
Fat thickness: 6 mm
Pinnation angle (°)
Depth (mm): 3 6
y (mm)
Median, First and Third quartiles
y direction
Fat thickness: 2 mm
Fat thickness: 6 mm
Pinnation angle (°)
Depth (mm): 3 6

Fig 6

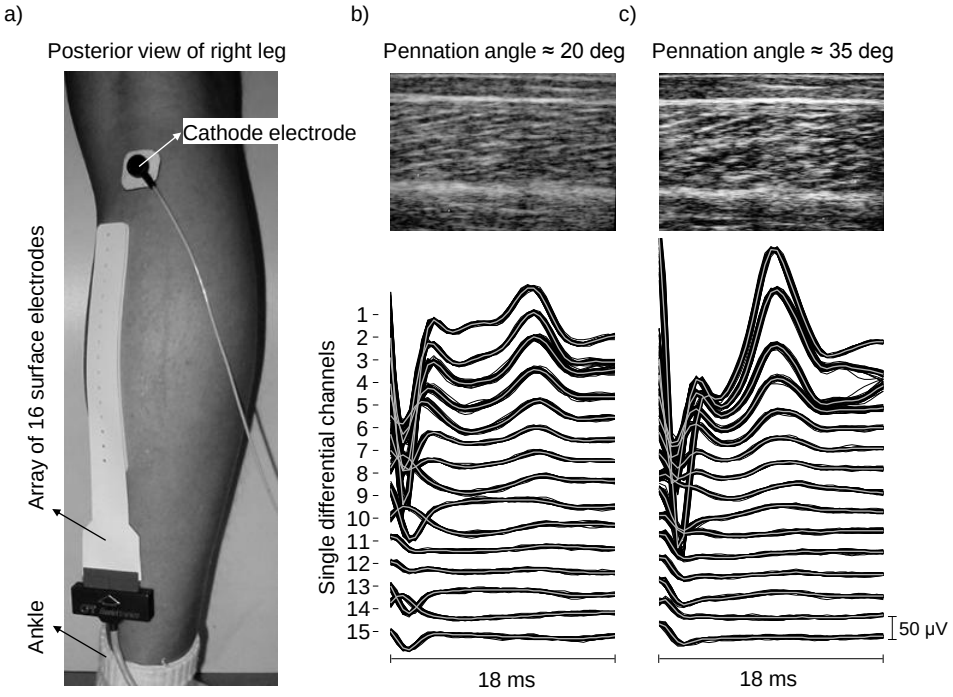
a)
Posterior view of right leg
Cathode electrode
Array of 16 surface electrodes
Ankle
b)
Pennation angle ≈ 20 deg
c)
Pennation angle ≈ 35 deg
Single differential channels
1
2
3
4
5
6
7
8
9
10
11
12
13
14
15
50 μV
18 ms
18 ms